Photocathode-assisted Redox Flow Desalination

Mengjun Liang[1#], Kuang Feng[2#], R. Karthick[1], Liguo Zhang[1], Yumeng Shi[3], Kwan San Hui[4], Kwun Nam Hui[5*], Feng Jiang[2*], Fuming Chen[1*]*

[1] Guangdong Provincial Key Laboratory of Quantum Engineering and Quantum Materials, Guangdong Provincial Engineering Technology Research Center for Wastewater Management and Treatment, School of Environment, School of Physics and Telecommunication Engineering, South China Normal University, Guangzhou 510006, P.R. China fmchen@m.scnu.edu.cn; zhanglg@scnu.edu.cn

[2] Institute of Semiconductor Science and technology, South China Normal University, Guangzhou 510631, China, fengjiangsolar@126.com

[3] International Collaborative Laboratory of 2D Materials for Optoelectronics Science and Technology of Ministry of Education, Institute of Microscale Optoelectronics, Shenzhen University, Shenzhen 518060, China

[4] Engineering, Faculty of Science, University of East Anglia, Norwich, UK

[5] Joint Key Laboratory of the Ministry of Education, Institute of Applied Physics and Materials Engineering, University of Macau, Avenida da Universidade, Taipa, Macau, PR China, bizhui@umac.mo

# these authors contributed equally

Abstract: The desalination techniques, such as reverse osmosis, distillation, capacitive deionization, and battery desalination, require lots of electrical or thermal energy consumption. Herein, we propose a consumption-free electrochemical desalination method based on the light-driven photocathode with Pt/CdS/Cu_2ZnSnS_4(CZTS)/Mo architecture. Modification of a CdS layer under CZTS can improve the desalination performance due to the inner p-n junction formed between CdS and CZTS that enhances the separation of the photoexcited carriers without recombination. This photocathode-assisted electrodialysis desalination plays the dual functions of both energy conversion and ion removal with the blocking of ion exchange membranes. The $[Fe(CN)_6]^{4-/3-}$ redox couples are recirculated between anode and photo-cathode as electrolyte while the salt streams are fed into middle compartment. Under light illumination, this architecture produces the photo-generated electrons to the redox couples with the conversion of $[Fe(CN)_6]^{3-}$ to $[Fe(CN)_6]^{4-}$ at the positive chamber, causing the cations capture in the presence of ion-exchange membrane. At the same time, $[Fe(CN)_6]^{4-}$ is oxidized at the negative reservoir. The light-driven electrochemical reaction of electrolyte redox couples can result in the continuous desalination process. This work will be significant for the consumption-free photoelectrochemical desalination research.

Keywords: Photo-desalination, electrochemical desalination, photo-cathode, Cu_2ZnSnS_4.

1. Introduction

The zero discharge of industrial wastewater is of the key importance nowadays, and the people's demand for fresh water resources is steadily increasing, which has become one of the world's challenges[1-9]. According to the estimation from World Health Organization (WHO), more than 20 % of world's population are facing the inadequate drinking water[10]. The ocean accounts for 97.3 % of the total water reserves on the earth[11]. To solve the crisis of freshwater, a lot of effort has been paid to seawater desalination. There are several methods adopted as the desalination technologies, such as multi-effect distillation (MED), multi-stage flash (MSF), reverse osmosis (RO), electrodialysis (ED) etc.[12-17] However, these technologies require the energy input like thermal or electrical energy, which is a burden in the era of energy shortage. For example, the energy expense of the matured RO, MSF or MED accounts for 50-77 % among the total cost [3, 18]. The energy consumption may critically affect the future of these technologies. It is necessary to look for the renewable energy supply to drive the desalt process. The direct photovoltaic desalination and solar thermal desalination have been widely investigated using the sustainable solar energy. In a photovoltaic (PV) desalination system, PV powered reverse osmosis (PV-RO) has emerged as a mature and commercially available technology which has been studied in depth [19-26]. In PV, the semiconductor p-n junction on the solar panel absorbs sunlight to form electron-hole pairs. Under the effect of the built-in electric field in the p-n junction, the holes flow from N region to the P region, and the electrons flow from the P region to the N region, forming a current output electric energy. RO is a pressure-driven desalination technology which consumes large energy. Thus, PV-RO desalination system uses PV power supply to solve the energy consumption problem in RO [27-29]. As for the solar thermal desalination, a solar thermal collector absorbs solar radiation and converts it into localized heat, leading to seawater evaporation [30-37] In general, a solar thermal evaporation desalination system contains two

layers: The top solar absorbing layer which has high absorption in the solar spectrum absorbs and converts the incident solar radiation into heat; The bottom thermal insulating layer which prevents the heat loss and increases the solar thermal efficiency is used to transport water to the surface heat region. For example, Kim et al. designed an efficient solar desalination device with a highly solar-to-vapor conversion efficiency of 91.8% under one sun illumination [38]. The device was constructed with a three-dimensional mesopores graphene network as the photo-absorber material at the top layer and a water-transporting layer (wood piece) as thermal insulation on the body. The mesopores in the photo-absorber material enhance the light absorption and help the generated vapors escape into the air. The wettable wood piece provides very efficient water paths by capillary force. Yin et al. developed a high-efficiency solar steam generation device with solar-to-vapor conversion efficiency of 91.5% under one sun illumination [39]. The designed device utilized macroporous double-network hydrogel of poly(ethylene glycol) diacrylate (PEGDA) and PANi as the light absorbing layer and the cellulose-wrapped layer served as both thermal insulation and water supply. Except for the direct photovoltaic desalination and solar thermal desalination, the photoelectrochemical desalination has emerged recently. For instance, Liang et al. proposed a bio-photo-electrochemical desalination cell with a bio-photocatalyst anode and $K_3[Fe(CN)_6]$ catholyte [40]. However, the salt can be intermittently removed due to the two separated electrodes, and an additional medium is required in order to avoid the bacteria growth on the anode. More recently, Kim et al. proposed the water-energy nexus technology [41], including the tri-functions of desalination, energy conversion and hydrogen production. The photo-generated charge carriers were produced by photo-anode with TiO_2 nano-rod arrays to facilitate the ion transportation, resulting in the desalination at middle salt compartment and the electricity production outside. However, there are still some issues in the system such as chloride oxidation, the pH value changes and the reduced energy efficiency etc. In our recent

work, we reported a photo-anode-based continuous desalination unit based on the redox reaction of 4-hydroxy-2, 2, 6, 6-tetramethylpiperidine 1-oxyl (TEMPO) [42], which consists of TiO_2 photoanode modified with LEG4 dye and TEMPO redox electrolyte. The salt removal rate (SRR) is very limited due to the low photocurrent but still serves as an important proof-of-concept for the continuous photo-desalination. Up till now, the photo-desalination based on photocathode hasn't been demonstrated yet. During the past few years, CZTS has been widely explored as the promising candidate for thin film solar cell because of its optimum band gap energy (1.5 eV) and high absorption coefficient (10^4 cm^{-1}) with a good absorption ability in the visible region [43, 44]. Moreover, CZTS is regarded as a low-cost, earth-abundant, toxic-element-free and sustainable photocatalyst with high light absorption and good stability [45, 46]. The combination of CdS layer and CZTS can form an internal p-n junction, which promotes the separation of photo-induced electrons and holes by the built-in electric field and thus improving the desalination performance [47].

In this work, we propose a photocathode-assisted redox-flow electrochemical desalination method by utilizing the light absorber CdS/CZTS as photocathode, carbon cloth coated with Pt nanoparticles as anode, $[Fe(CN)_6]^{4-}/[Fe(CN)_6]^{3-}$ as redox electrolyte. The reduction of ferricyanide happens with the cation extraction from the near salt stream through cation ion exchange membrane which is driven by CdS/CZTS photocathode, while the anions in the diluted stream are transferred to other concentrated salt stream through anion ion exchange membrane, resulting in the desalination. This present work can achieve the continuous desalination by circulating the redox flow electrolyte based on the CdS/CZTS photocathode illumination. Deposition of a CdS layer on CZTS can form an inner p-n junction at the interface of CdS/CZTS which not only enhances the separation rate of photoexcited carriers but also reduces surface recombination, and thus generally enhancing photocathode performance. This new consumption-free electrochemical desalination method based on the

light-driven photocathode with Pt/CdS/CZTS/Mo architecture was firstly proposed which might open up an avenue for energy-free desalination based on the photocathode illumination, and will further motivate the development of photocathode materials to enhance the electrochemical desalination performance.

2. Materials and methods

2.1 Materials and Fabrication of photocathode

The specifications of chemicals in this work can be given as follows: $SC(NH_2)_2$ (Macklin, 99%), $Cu(NO_3)_2$ (Macklin, 99.99%), $Zn(NO_3)_2$ (Aladdin, 99.99%), $Sn(CH_3SO_3)_2$ (Macklin, 50 wt. % in H_2O), HNO_3 (Macklin, 98%), $CdSO_4$ (Macklin, 99%), NH_4OH (Macklin, 25-28%), H_2PtCl_6 (Macklin, 99.995%), $K_3Fe(CN)_6$ (Energy Chemical, 99%), $K_4Fe(CN)_6 \cdot 3H_2O$ (Macklin, ⩾99.5%) and NaCl (Aldrich, 99.5%). All these reagents were analytical grade and used without any purification. The water solution used in the experiment was prepared using deionized water.

The preparation process of the photocathode was reported elsewhere[48-50]. In brief, the first layer of CZTS thin film was prepared using 50 mM thiourea, 17 mM copper nitrate, 11.5 mM zinc nitrate, and 11.5 mM tin methanesulfonate as precursor in aqueous condition. The pH value was adjusted to 1.5 using nitric acid before spraying onto Mo-coated soda-lime glass substrate (Mo/glass) that was preheated for 10 min at 380 ℃. Finally, the obtained CZTS thin film was further sulfurized using sulphur powder source at 600 ℃ for 30 min. The second layer of CdS film was deposited using the chemical bath deposition method (CBD) as follows: as-synthesized CZTS film was dipped into an aqueous solution of 12.5 mM $CdSO_4$, 0.22 mM $SC(NH_2)_2$, and 11 M NH_4OH for 13 min at 60 ℃. The final catalyst layer of Pt particles was deposited on the CdS/CZTS films by photoelectrodeposition. The deposition was conducted

using a three-electrode electrochemical system with CdS/CZTS as working electrode, Pt sheet as counter electrode, Ag/AgCl as reference electrode in 0.1 M Na_2SO_4 solution containing 1 mM H_2PtCl_6 as electrolyte. During the deposition process, the working electrode was illuminated by the simulated AM 1.5G solar irradiation with 300 W Xenon lamp for 30 seconds.

2.2 Fabrication of PC-ED device (photocathode electrochemical desalination)

The PC-ED cell comprises two redox streams (RS), two salt streams (SS), photocathode (PC) and counter electrodes (CE). The configuration is sequenced as follows:

PC | RS || SS || SS || RS | CE

where "|" denotes the separation of components, and "||" represents the membranes which play an important role in the effective separation of molecules[51, 52], i.e., anion exchange membrane (AEM) or cation exchange membrane (CEM). One AEM was inserted between the two salt streams A and B as shown in Figure 1a. Two CEMs were placed between redox flow and salt streams. The redox electrolyte contains a mixture of 40 mM of potassium ferrocyanide and potassium ferricyanide with the addition of 2000 ppm of NaCl. The salt stream contains the same concentration of NaCl as that in the redox chambers.

The anode and cathode chambers were both fed with ferri-/ferrocyanide solution with concentration of 40/40 mM. The electrolytes were prepared by dissolving $K_3Fe(CN)_6$ and $K_4Fe(CN)_6 \cdot 3H_2O$ with a mole ratio of 1:1 in a 2000 ppm NaCl solution. The total volume was 4 ml. The desalination and concentrate chambers (A and B) were fed with the same concentrations of NaCl with 2000 ppm as initial salt feeds and each volume was 1.35 ml. The thickness of each plate was 3 mm. In the centre of this compartment, the square-cut area exposed to the electrolyte was about 1 cm^2, which was the active membrane area applied. The

tube with 1 mm diameter was applied in the tests, and the flow rates were controlled at 4.15 ml/min.

2.3 The tests of electrochemistry, photo-electrochemistry and desalination

The electrochemical measurements of cyclic voltammetry (CV) and electrochemical impedance spectroscopy (EIS) were conducted by an electrochemical working station (CHI760E) with a conventional three-electrode system. Glassy carbon, Pt sheet and Ag/AgCl electrodes are served as working electrode, counter electrode and reference electrode, respectively, and 40 mM/40 mM $[Fe(CN)_6]^{4-}$/$[Fe(CN)_6]^{3-}$ solution containing 2000 ppm NaCl as electrolyte. The linear sweep voltammetry (LSV) was also tested with three electrodes, whereas the selected working electrode was photocathode material (CdS/CZTS), the other two electrodes and electrolyte were same as CV and EIS tests. The photo-driven discharge of PC-ED at zero bias was conducted by CHI760E Potentiostat with I-t program. The photo-driven discharge of PC-ED with the constant current was measured by NEWARE Battery Testing System. The flow rate of salt and redox solution was controlled by peristaltic pump (NKCP-C-S04B). The conductivity of the salt concentration was monitored by conductivity meters (eDAQ, EPU357). The controllable wavelength of 400-800 nm was used as the continuous light source from A YSL Photonics SC-Pro, and a concave lens was located between the light source and the device to enlarge the light spot in order to cover the whole photocathode. The light source output spectrum was measured by a spectrometer (Maya2000 Pro, Ocean Optics).

3. Results and discussion

The SEM scan was conducted for the surface morphology of CdS/CZTS as shown in Figure S1. It was clearly observed that CdS is well covered on the surface of CZTS grains [49].

Figure S2 demonstrates the photograph of photocathode electrochemical desalination (PC-ED) device set-up with illumination and Figure 1a shows the schematic configuration for PC-ED device. The PC-ED device consists of four compartments, three membranes and two electrodes. The $[Fe(CN)_6]^{4-/3-}$ redox couples are recirculated using a peristaltic pump in negative and positive chambers. The other two middle compartments are fed with salt streams (stream A & stream B), and circulated individually. The salt stream A and stream B are separated by anion exchange membrane (AEM) and two cation exchange membranes (CEM) are placed between salt streams and the redox-flow chambers. The mechanism of photocathode is displayed in Figure 1b. Upon illumination, CZTS photo active material is excited and generated the electrons at conduction band (CB), followed by electrons acceptance by the nearby n-type semiconductor CdS and tunnelling to Pt layer that expedites the reduction of ferricyanide ion. Simultaneously, the sodium ions in stream A are coupling extracted to photo-cathode chamber through CEM in order to compensate the static balance while chloride ions are transmitted to stream B through AEM. The extracted sodium ions are carried to the anode compartment together with the redox couples. With the further oxidation back to ferricyanide, the sodium ions in anode chamber are released to stream B. In the outside circuit, the electrons from the anode collector are provided to the excited state of CZTS holes via the conducting Mo layer. The overall effect is that the salt in stream A is removed to stream B under the light illumination on the CdS/CZTS cathode.

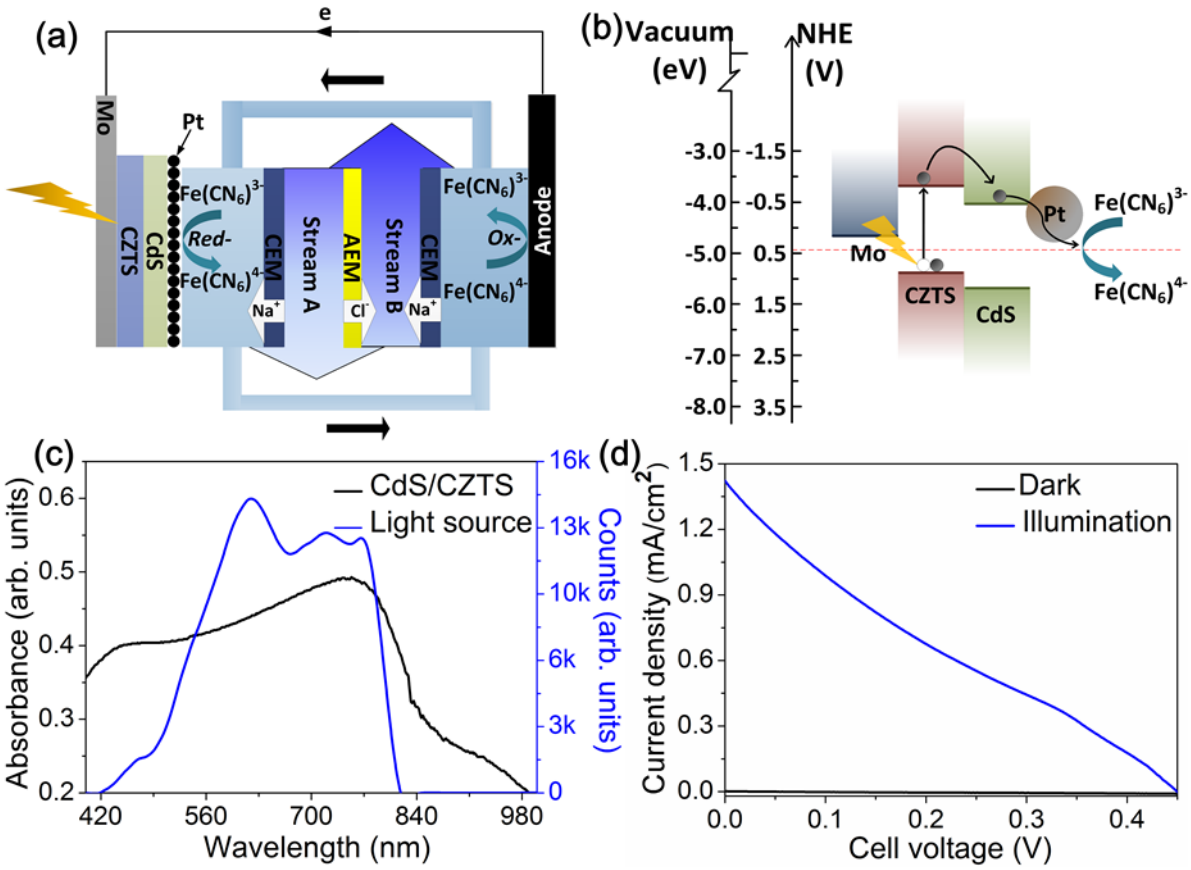

Figure 1: (a) The schematic diagram of PC-ED device; (b) The internal reaction mechanism of photocathode; (c) The absorption spectra of photocathode and light source; (d) The I-V curves of CdS/CZTS electrode under dark and 153 mW/cm^2 illumination.

Figure 1c shows the absorption spectra of CdS/CZTS and the continuous wavelength light source output spectrum with the range of 400-1000 nm. The CdS/CZTS absorption spectra overlap well with the light source spectrum between 420 nm and 800 nm. Therefore, the sufficient photons will be absorbed by CdS/CZTS layers in this research. The I-V curves of CdS/CZTS with/without illumination are demonstrated in Figure 1d. The current density can reach 1.4 mA/cm^2 under light irradiation with power of 153 mW. However, the current density is close to zero in the dark condition. The obtained photocurrent can be used for the continuous electrochemical desalination.

To investigate the redox reaction of $[Fe(CN)_6]^{4-/3-}$ couples, the CV technique is utilized by the electrochemical working station with the glassy carbon as working electrode, Pt sheet as counter electrode and Ag/AgCl as reference electrode in an aqueous medium that contains the 40 mM/40 mM of $[Fe(CN)_6]^{4-/3-}$ redox couples and 2000 ppm of NaCl. As shown in Figure 2a, a pair of redox peaks are assigned to oxidation at 0.45 V and reduction at 0.07 V. According to the Nernst Equation (1)[53]:

$$E_{redox} = E^0{}_{redox} + \frac{RT}{nF} \ln\left[\frac{C_{ox}}{C_{red}}\right] \qquad (1)$$

where C_{ox} and C_{red} are concentrations of $[Fe(CN)_6]^{3-}$ and $[Fe(CN)_6]^{4-}$. During the desalination process, the concentration of $[Fe(CN)_6]^{3-}$ is equal to the concentration of $[Fe(CN)_6]^{4-}$. Thus, $E_{redox} = E^0{}_{redox} \approx E_{1/2}$. Furthermore, the standard hydrogen electrode (SHE) appears at -4.5 eV at the vacuum level, and the relationship between the redox potential E_{redox} and the Fermi level $E_{F,\,redox}$ can be presented in the below equation (2)[54]:

$$E_{F,redox} = -4.5\ \text{eV} - e_o E_{redox} \qquad (2)$$

Combined Eq. (1-2) and CV curve, $E_{redox} = E_{\frac{1}{2}} = 0.26\,V$, e_o = 1 (electron), the fermi level of the redox couple is found to be $E_{F,redox} = -4.76\,eV$, that matches well with the energy band of CdS/CZTS as an efficient charge transfer.

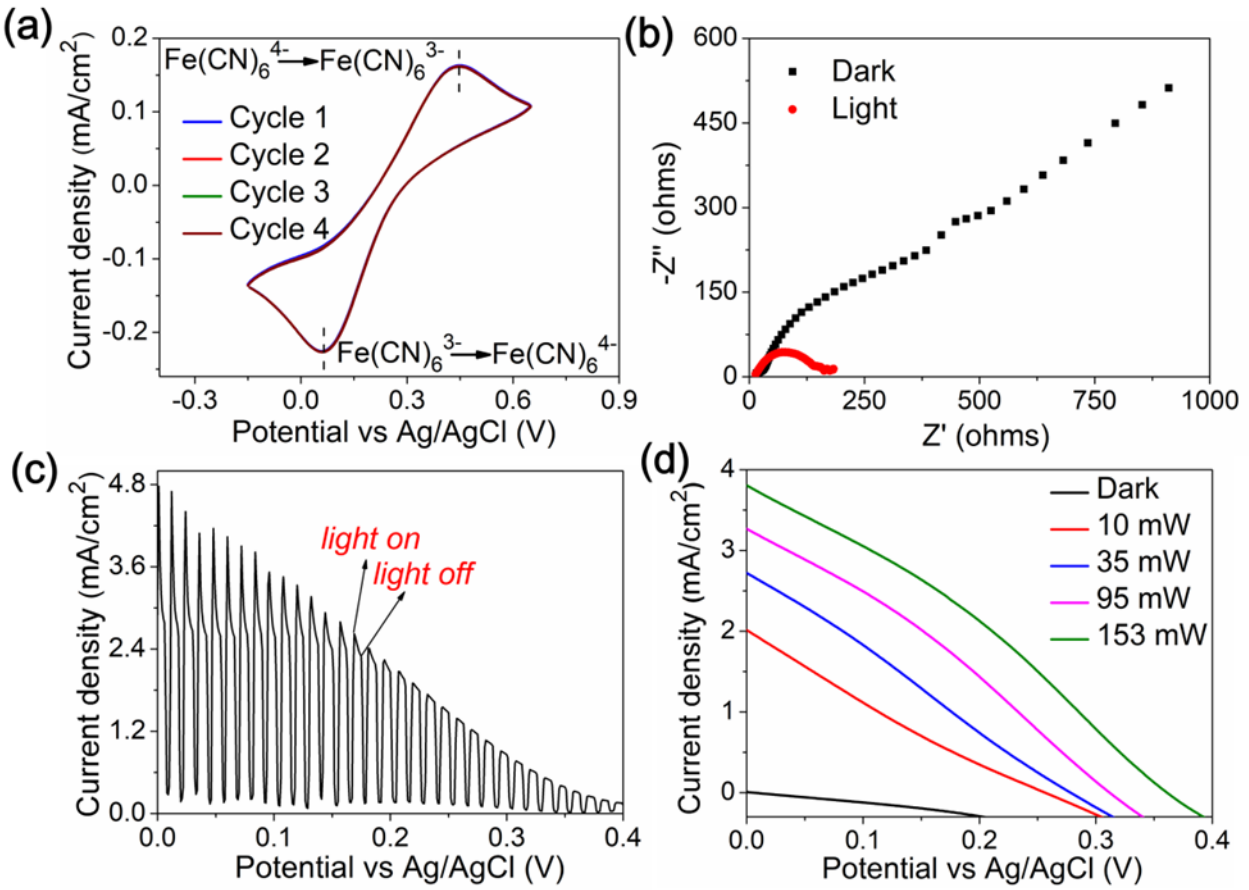

Figure 2: (a) The three-electrodes CV of $[Fe(CN)_6]^{4-/3-}$ with scanning rate of 10 mV/s; (b) EIS spectrum of CdS/CZTS recorded from 100 kHz to 1 Hz at zero bias; LSV curve of CdS/CZTS electrode under 153 mW/cm^2 chopped illumination (c) and under different intensities of the output power density (d).

To understand the charge transfer kinetics, the EIS was carried out using three electrodes. As shown in Figure 2b, the photocathode material has a smaller semi-circle on the EIS Nyquist diagram under light illumination, compared with the dark condition. This indicates the lower surface resistance, caused by the photo-induced carriers. Moreover, the photoelectrochemical properties of CdS/CZTS photoelectrodes were further determined by LSV under 153 mW/cm^2 chopped illumination (Figure 2c). It is observed that the photocurrent difference between light and dark conditions is larger at the zero potential vs

Ag/AgCl. The photocurrent obtained under light conditions can be used for desalination. Figure 2d shows the effect of the power density of the light source on the photocurrent density. The specific photocurrent densities are 2, 2.7, 3.3 and 3.8 mA/cm^2 at 0 V vs Ag/AgCl with the specific power densities of 10, 35, 95 and 153 mW/cm^2, respectively. Among the tested batch, the highest photocurrent can be obtained at the power density of 153 mW/cm^2. Thus, this power density is chosen for further desalination.

Figure 3a shows the variation of photocurrent intensity at zero bias under 153 mW/cm^2 illumination. It can be seen that after turning on the light, the photocurrent immediately jumped to 0.47 mA/cm^2, then gradually decreased from 0.25 mA/cm^2 with the prolongation of time. At the same time, the salt concentrations of the two salt channels (stream A & stream B) were recorded by conductivity meters, as shown in Figure 3b. The salt conductivity decreases from the initial 4143 uS/cm to 2866 uS/cm in stream A. The charge efficiency and salt removal rate are 0.64 and 1.06 $\mu g \cdot cm^{-2} \cdot min^{-1}$, respectively. At the same time, the salt conductivity in stream B increases from 4136 uS/cm to 6081 uS/cm. Thus, the salt in stream A is removed to stream B, which is driven by the photo-illumination. The relatively weak photocurrent results in a poor desalination performance which is affected by many factors such as ions exchange membranes, electrodes surface areas, the thickness of device as well as some other uncontrollable factors etc. Currently, we are working on some strategies to improve the photocurrent and desalination performance.

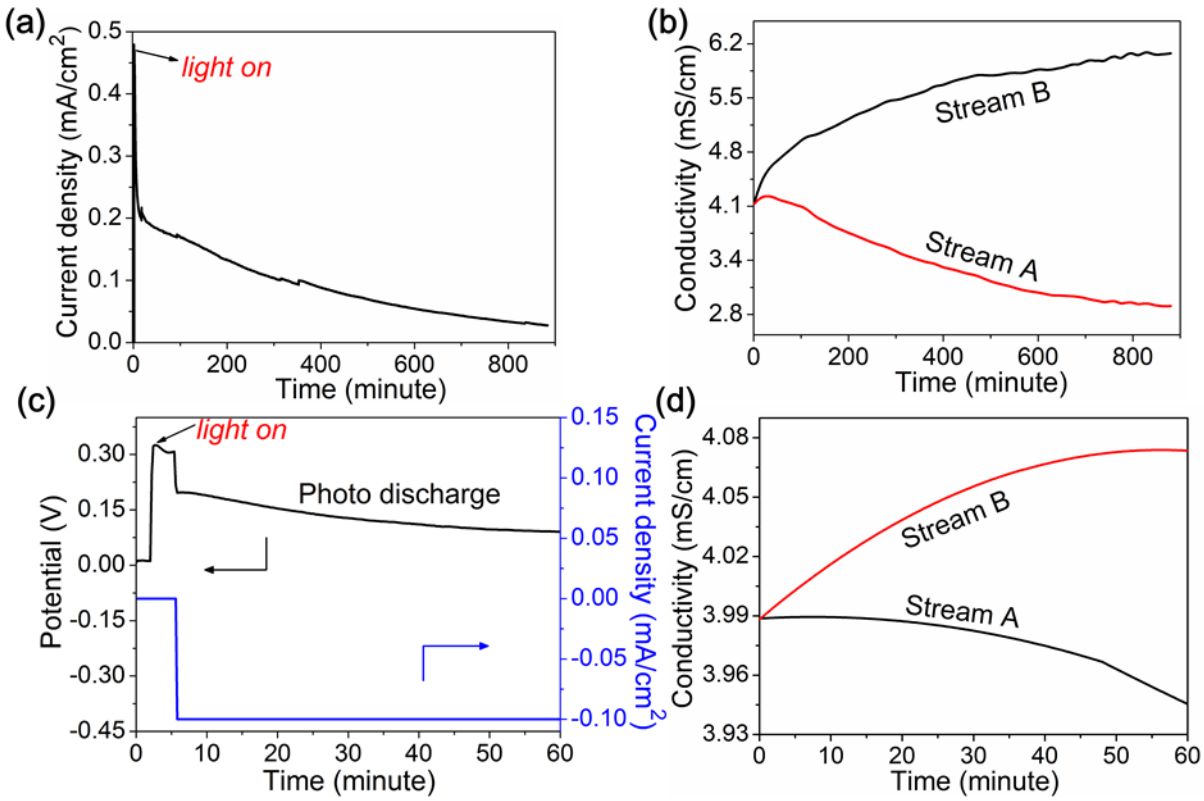

Figure 3: (a) Photo-driven current density at zero bias (short circuit) and (b) its corresponding conductivity variation; (c) Photo-driven discharge curve at 0.1 mA/cm^2 constant current density and (d) its corresponding conductivity variation.

The photocatalytic desalination mechanism of PC-ED device can be described as follows;

$$h\upsilon + CdS/CZTS \rightarrow e^-_{(Pt)} + K_3[Fe(CN)_6]^{3-} \rightarrow K_3(Na)[Fe(CN)_6]^{4-} \quad (3)$$

$$Na^+_{(Salt\ Stream\ A)} \xrightarrow{CEM} K_3(Na)[Fe(CN)_6]^{4-} \quad (4)$$

$$K_3(Na)[Fe(CN)_6]^{4-} \rightarrow K_3[Fe(CN)_6]^{3-} + e^-_{(IE)} + Na^+ \quad (5)$$

$$Excess(Na^+) \xrightarrow{CEM} Salt\ Stream\ B \quad (6)$$

$$Cl^-_{(Salt\ Stream\ A)} \xrightarrow{AEM} Salt\ Stream\ B \quad (7)$$

Figure 3c shows the voltage curve under the discharge of 0.1 mA/cm^2 constant current density, which was recorded with the battery tester. On the light illumination, the open-circuit

voltage (OCV) can reach 0.32 V immediately. Once applying the discharge current of 0.1 mA/cm^2, the voltage drops to 0.20 V and keeps decreasing gradually with the desalination process and the energy consumption of desalination cell. The salt conductivity is recorded in Figure 3d during the photo-discharge. The conductivity decreases from the initial 3988 uS/cm to 3945 uS/cm in stream A. The charge efficiency and salt removal rate are 0.16 and 0.52 $\mu g \cdot cm^{-2} \cdot min^{-1}$, respectively. The salt conductivity in stream B rises from the initial 3982 uS/cm to 4073 uS/cm after 60 minutes. There are some differences of conductivity change in stream A and stream B which may be due to the short desalination and small photo-current. Specifically, the desalination system is not stable at the initial stage, especially under the condition of small photocurrent. In the case of photo-driven desalination at zero bias (short circuit) in Figure 3a-b, the photocurrent is larger, and thus the desalination effect is more obvious, and the desalination time reaches 14.7 hours. However, a small constant current density with the value of 0.1 mA/cm^2 is applied, which is smaller than that at the zero bias. Hence, the desalination effect is poor in Figure 3c-d, only lasting for 60 minutes. Actually, in the initial stage of short-circuit desalination in Figure 3b, the variation of salt concertation is also unstable. However, with the long desalination process, the change of salt concertation tends to be stable.

4. Conclusion

A photocathode-assisted redox-flow electrochemical desalination method was proposed. CdS/CZTS photocathode can be excited under illumination and transport electrons to ferricyanide ions through platinum layer for reduction reaction. The reduced ferrocyanide ions carrier the sodium ions and flow to anode channel where the sodium ions are extracted by the salt stream B due to the oxidation of redox couples. The redox reaction is accompanied by the transport of sodium and chloride ions in the two salt streams (desalinated salt stream A

and salinated salt stream B). This photocathode-assisted redox flow electrochemical system can achieve the continuous desalination by circulating the redox flow electrolyte. This new method can open up an avenue for energy-free desalination based on the photocathode illumination, and will further motivate the development of photocathode materials to enhance the electrochemical desalination performance.

Acknowledgements

This project was supported by South China Normal University, the SCNU Outstanding Young Scholar Project (8S0256, 8S0103), the Scientific and Technological Plan of Guangdong Province (2018A050506078), Key-Area Research and Development Program of Guangdong Province (2019B110209002), and National Natural Science Foundation of China (51978290, 61704060). F. Chen acknowledges the Pearl River Talent Program (2019QN01L951).

Conflict of interest

The authors declare no conflict of interest

REFERENCES

1. M. Gao, L. Zhu, C. K. Peh and G. W. Ho, *Energy & Environmental Science*, 2019, **12**, 841-864.
2. L. Zhu, M. Gao, C. K. N. Peh and G. W. Ho, *Nano Energy*, 2019, **57**, 507-518.
3. S. Burn, M. Hoang, D. Zarzo, F. Olewniak, E. Campos, B. Bolto and O. Barron, *Desalination*, 2015, **364**, 2-16.
4. H. M. N. AlMadani, *Renewable Energy*, 2003, **28**, 1915-1924.
5. M. Khayet, *Desalination*, 2013, **308**, 89-101.
6. Y. Zhang, X. Cheng, X. Jiang, J. J. Urban, C. H. Lau, S. Liu and L. Shao, *Materials Today*, 2020.
7. F. You, Y. Xu, X. Yang, Y. Zhang and L. Shao, *Chemical communications*, 2017, **53**, 6128-6131.
8. Y. Q. Zhang, X. B. Yang, Z. X. Wang, J. Long and L. Shao, *J. Mater. Chem. A*, 2017, **5**, 7316-7325.
9. L. Mao, L. Zhang, N. Gao and A. Li, *Green Chemistry*, 2013, **15**, 727.

10. M. R. Qtaishat and F. Banat, *Desalination*, 2013, **308**, 186-197.
11. K. N. Knust, D. Hlushkou, R. K. Anand, U. Tallarek and R. M. Crooks, *Angew Chem Int Ed Engl*, 2013, **52**, 8107-8110.
12. T. Kim, C. A. Gorski and B. E. Logan, *Environmental Science & Technology Letters*, 2017, **4**, 444-449.
13. Y. Ghalavand, M. S. Hatamipour and A. Rahimi, *Desalination and Water Treatment*, 2014, 1-16.
14. T. A. H. Ratlamwala, I. Dincer and M. A. Gadalla, *International Journal of Energy Research*, 2013, **37**, 1569-1579.
15. J. Lee, S.-H. Yu, C. Kim, Y.-E. Sung and J. Yoon, *Physical Chemistry Chemical Physics*, 2013, **15**, 7690-7695.
16. W.-T. Gao, Q. Chen, M.-G. Du, W.-M. Zhang, C.-Y. Cao and W.-G. Song, *Green Chemistry*, 2020, **22**, 2213-2224.
17. G. Li, W.-C. Law and K. C. Chan, *Green Chemistry*, 2018, **20**, 3689-3695.
18. S. Lattemann, M. D. Kennedy, J. C. Schippers and G. Amy, *Sustainability Science and Engineering*, Elsevier B.V., 2010.
19. M. Freire-Gormaly and A. M. Bilton, *Renewable Energy*, 2019, **135**, 108-121.
20. C.-S. Karavas, K. G. Arvanitis and G. Papadakis, *Desalination*, 2019, **466**, 97-106.
21. M. T. Mito, X. Ma, H. Albuflasa and P. A. Davies, *Renewable and Sustainable Energy Reviews*, 2019, **112**, 669-685.
22. S. M. Shalaby, *Renewable and Sustainable Energy Reviews*, 2017, **73**, 789-797.
23. B. Wu, A. Maleki, F. Pourfayaz and M. A. Rosen, *Solar Energy*, 2018, **163**, 91-103.
24. H. Rezk, E. T. Sayed, M. Al-Dhaifallah, M. Obaid, A. H. M. El-Sayed, M. A. Abdelkareem and A. G. Olabi, *Energy*, 2019, **175**, 423-433.
25. M. A. Alghoul, P. Poovanaesvaran, M. H. Mohammed, A. M. Fadhil, A. F. Muftah, M. M. Alkilani and K. Sopian, *Renewable Energy*, 2016, **93**, 101-114.
26. A. M. Delgado-Torres, L. García-Rodríguez and M. J. del Moral, *Desalination*, 2020, **477**, 114247.
27. F. E. Ahmed, R. Hashaikeh and N. Hilal, *Desalination*, 2019, **453**, 54-76.
28. K. Q. Peng and S. T. Lee, *Adv Mater*, 2011, **23**, 198-215.
29. C. Cho, K. Nam, G. Y. Kim, Y. H. Seo, T. G. Hwang, J. W. Seo, J. P. Kim, J. I. Han and J. Y. Lee, *Scientific reports*, 2019, **9**, 18999.
30. M. Gao, L. Zhu, C. K. Peh and G. W. Ho, *Energy and Environmental Science*, 2019, **12**, 841-864.
31. L. Zhu, M. Gao, C. K. N. Peh and G. W. Ho, *Nano Energy*, 2019, **57**, 507-518.
32. P. Tao, G. Ni, C. Song, W. Shang, J. Wu, J. Zhu, G. Chen and T. Deng, *Nature Energy*, 2018, **3**, 1031-1041.
33. L. Zhu, M. Gao, C. K. N. Peh, X. Wang and G. W. Ho, *Advanced Energy Materials*, 2018, **8**, 1702149.
34. C. Chen, Y. Kuang and L. Hu, *Joule*, 2019, **3**, 683-718.
35. Y. Zhang, T. Xiong, D. K. Nandakumar and S. C. Tan, 2020, **7**, 1903478.
36. Y. Zhang, S. K. Ravi, L. Yang, J. V. Vaghasiya, L. Suresh, I. Tan and S. C. Tan, *ACS Applied Materials & Interfaces*, 2019, **11**, 38674-38682.
37. Y. Zhang, S. K. Ravi and S. C. Tan, *Nano Energy*, 2019, **65**, 104006.
38. K. Kim, S. Yu, C. An, S. W. Kim and J. H. Jang, *ACS applied materials & interfaces*, 2018, **10**, 15602-15608.
39. X. Yin, Y. Zhang, Q. Guo, X. Cai, J. Xiao, Z. Ding and J. Yang, *ACS applied materials & interfaces*, 2018, **10**, 10998-11007.
40. Y. Liang, H. Feng, D. Shen, N. Li, Y. Long, Y. Zhou, Y. Gu, X. Ying and Q. Dai, *Electrochimica Acta*, 2016, **202**, 197-202.
41. S. Kim, G. Piao, D. S. Han, H. K. Shon and H. Park, *Energy & Environmental Science*, 2018, **11**, 344-353.

42. F. Chen, R. Karthick, Q. Zhang, J. Wang, M. Liang, J. Dai, X. Jiang and Y. Jiang, *Journal of Materials Chemistry A*, 2019, **7**, 20169-20175.
43. T. H. Nguyen, T. Kawaguchi, J. Chantana, T. Minemoto, T. Harada, S. Nakanishi and S. Ikeda, *ACS applied materials & interfaces*, 2018, **10**, 5455-5463.
44. F. Jiang, S. Li, C. Ozaki, T. Harada and S. Ikeda, *Solar RRL*, 2018, **2**, 1700205.
45. T. H. Nguyen, S. Fujikawa, T. Harada, J. Chantana, T. Minemoto, S. Nakanishi and S. Ikeda, *ChemSusChem*, 2016, **9**, 2414-2420.
46. B. Shin, O. Gunawan, Y. Zhu, N. A. Bojarczuk, S. J. Chey and S. Guha, *Progress in Photovoltaics: Research and Applications*, 2013, **21**, 72-76.
47. K. Wang, D. Huang, L. Yu, H. Gu, S. Ikeda and F. Jiang, *Journal of colloid and interface science*, 2019, **536**, 9-16.
48. H. Zhang, B. Qin, J. Han and S. Passerini, *ACS Energy Letters*, 2018, **3**, 1769-1770.
49. K. Feng, D. Huang, L. Li, K. Wang, J. Li, T. Harada, S. Ikeda and F. Jiang, *Applied Catalysis B: Environmental*, 2020, **268**, 118438.
50. F. Jiang, S. Li, C. Ozaki, T. Harada and S. Ikeda, *Solar RRL* 2018, **2**, 1700205.
51. Y. Zhang, J. Ma and L. Shao, *Journal of Materials Chemistry A*, 2020, **8**, 5078-5085.
52. M. Razali, J. F. Kim, M. Attfield, P. M. Budd, E. Drioli, Y. M. Lee and G. Szekely, *Green Chemistry*, 2015, **17**, 5196-5205.
53. N. Elgrishi, K. J. Rountree, B. D. McCarthy, E. S. Rountree, T. T. Eisenhart and J. L. Dempsey, *Journal of Chemical Education*, 2017, **95**, 197-206.
54. K. Rajeshwar, *Encyclopedia of electrochemistry*, 2007, **6**, 1-53.

The table of contents entry: A consumption-free electrochemical desalination method is demonstrated to work based on the light-driven photocathode with Pt/CdS/CZTS/Mo architecture.

Keywords: Photo-desalination, electrochemical desalination, photo-cathode, Cu_2ZnSnS_4

M. Liang, K. Feng, R. Karthick, L. Zhang, Y. Shi, K. S. Hui, K. N. Hui, F.Jiang, F. Chen

Photocathode-assisted Redox Flow Desalination

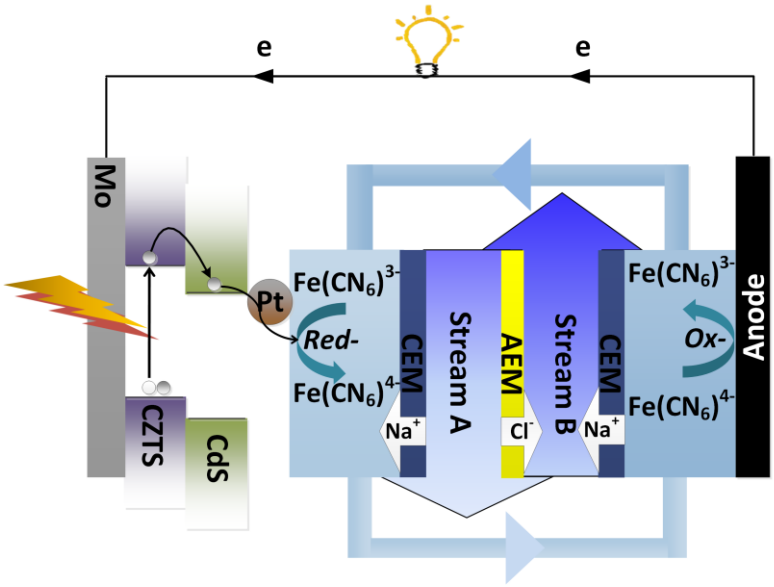

Column Title: M. Liang et al